

Euclid Quick Data Release (Q1) – Ultracool dwarfs in the Euclid Deep Field North ★

A. Mohandas^{★1}, R. L. Smart^{2,3}, C. Reylé¹, V. Le Brun⁴, A. Pérez-Garrido⁵, E. Bañados⁶, B. Goldman^{7,8},
H. R. A. Jones³, S. L. Casewell⁹, M. R. Zapatero Osorio¹⁰, T. Dupuy¹¹, M. Rejkuba¹², E. L. Martín^{13,14},
C. Dominguez-Tagle^{13,14}, M. Žerjal^{13,14}, N. Huélamo¹⁰, N. Lodieu^{15,14}, P. Cruz¹⁰, R. Rebolo^{13,16,14}, M. W. Phillips¹¹,
J.-Y. Zhang^{13,14}, N. Aghanim¹⁷, B. Altieri¹⁸, A. Amara¹⁹, S. Andreon²⁰, N. Auricchio²¹, C. Baccigalupi^{22,23,24,25},
M. Baldi^{26,21,27}, A. Balestra²⁸, S. Bardelli²¹, P. Battaglia²¹, A. Biviano^{23,22}, A. Bonchi²⁹, E. Branchini^{30,31,20},
M. Brescia^{32,33}, J. Brinchmann^{34,35}, S. Camera^{36,37,2}, G. Cañas-Herrera^{38,39,40}, V. Capobianco², C. Carbone⁴¹,
J. Carretero^{42,43}, S. Casas⁴⁴, M. Castellano⁴⁵, G. Castignani²¹, S. Cavuoti^{33,46}, K. C. Chambers⁴⁷, A. Cimatti⁴⁸,
C. Colodro-Conde¹³, G. Congedo¹¹, C. J. Conselice⁴⁹, L. Conversi^{50,18}, Y. Copin⁵¹, A. Costille⁴, F. Courbin^{52,53},
H. M. Courtois⁵⁴, M. Cropper⁵⁵, A. Da Silva^{56,57}, H. Degaudenzi⁵⁸, G. De Lucia²³, H. Dole¹⁷, M. Douspis¹⁷,
F. Dubath⁵⁸, X. Dupac¹⁸, S. Dusini⁵⁹, S. Escoffier⁶⁰, M. Farina⁶¹, F. Faustini^{45,29}, S. Ferriol⁵¹, S. Fotopoulou⁶²,
M. Frailis²³, E. Franceschi²¹, S. Galeotta²³, K. George⁶³, W. Gillard⁶⁰, B. Gillis¹¹, C. Giocoli^{21,27}, J. Gracia-Carpio⁶⁴,
B. R. Granett²⁰, A. Grazian²⁸, F. Grupp^{64,63}, S. V. H. Haugan⁶⁵, J. Hoar¹⁸, W. Holmes⁶⁶, I. M. Hook⁶⁷, F. Hormuth⁶⁸,
A. Hornstrup^{69,70}, K. Jahnke⁶, M. Jhabvala⁷¹, E. Keihänen⁷², S. Kermiche⁶⁰, A. Kiessling⁶⁶, B. Kubik⁵¹, K. Kuijken⁴⁰,
M. Kümmel⁶³, M. Kunz⁷³, H. Kurki-Suonio^{74,75}, Q. Le Boulc’h⁷⁶, A. M. C. Le Brun⁷⁷, D. Le Mignant⁴, S. Ligorì²,
P. B. Lilje⁶⁵, V. Lindholm^{74,75}, I. Lloro⁷⁸, G. Mainetti⁷⁶, D. Maino^{79,41,80}, E. Maiorano²¹, O. Mansutti²³, S. Marcin⁸¹,
O. Marggraf⁸², M. Martinelli^{45,83}, N. Martinet⁴, F. Marulli^{84,21,27}, R. Massey⁸⁵, E. Medinaceli²¹, S. Mei^{86,87},
Y. Mellier^{88,89}, M. Meneghetti^{21,27}, E. Merlin⁴⁵, G. Meylan⁹⁰, A. Mora⁹¹, M. Moresco^{84,21}, L. Moscardini^{84,21,27},
R. Nakajima⁸², C. Neissner^{92,43}, S.-M. Niemi³⁸, C. Padilla⁹², S. Paltani⁵⁸, F. Pasian²³, K. Pedersen⁹³,
W. J. Percival^{94,95,96}, V. Pettorino³⁸, S. Pires⁹⁷, G. Polenta²⁹, M. Poncet⁹⁸, L. A. Popa⁹⁹, L. Pozzetti²¹, F. Raison⁶⁴,
A. Renzi^{100,59}, J. Rhodes⁶⁶, G. Riccio³³, E. Romelli²³, M. Roncarelli²¹, R. Saglia^{63,64}, Z. Sakr^{101,102,103}, D. Sapone¹⁰⁴,
B. Sartoris^{63,23}, J. A. Schewtschenko¹¹, M. Schirmer⁶, P. Schneider⁸², T. Schrabback¹⁰⁵, A. Secroun⁶⁰, G. Seidel⁶,
S. Serrano^{106,107,108}, P. Simon⁸², C. Sirignano^{100,59}, G. Sirri²⁷, L. Stanco⁵⁹, J. Steinwagner⁶⁴, C. Surace⁴,
P. Tallada-Crespí^{42,43}, A. N. Taylor¹¹, I. Tereno^{56,109}, R. Toledo-Moreo¹¹⁰, F. Torradeflot^{43,42}, A. Tsyganov¹¹¹,
I. Tutusaus¹⁰², L. Valenziano^{21,112}, J. Valiviita^{74,75}, T. Vassallo^{63,23}, G. Verdoes Kleijn¹¹³, A. Veropalumbo^{20,31,30},
D. Vibert⁴, Y. Wang¹¹⁴, J. Weller^{63,64}, A. Zacchei^{23,22}, G. Zamorani²¹, F. M. Zerbi²⁰, E. Zucca²¹, J. Martín-Fleitas⁹¹,
and V. Scottez^{88,115}

(Affiliations can be found after the references)

March 31, 2025

ABSTRACT

Ultracool dwarfs (UCDs) encompass the lowest-mass stars and brown dwarfs, defining the stellar-substellar boundary. They have significant potential for advancing the understanding of substellar physics; however, these objects are challenging to detect due to their low luminosity. The wide coverage and deep sensitivity of the *Euclid* survey will increase the number of confirmed and well-characterised UCDs by several orders of magnitude. In this study, we take advantage of the *Euclid* Quick Data Release (Q1) and in particular we look in detail at the known and new UCDs in the *Euclid* Deep Field North (22.9 deg² down to $J_E \approx 24.5$ mag), to understand the advantages of using the slitless *Euclid* spectroscopy.

We compile a comparison sample of known UCDs and use their spectra to demonstrate the capability of *Euclid* to derive spectral types using a template-matching method. This method is then applied to the spectra of the newly identified candidates. We confirm that 33 of these candidates are new UCDs, with spectral types ranging from M7 to T1 and $J_E = 17\text{--}21$ mag. We look at their locus in colour-colour diagrams and compare them with the expected colours of QSOs. A machine-readable catalogue is provided for further study, containing both the comparison sample and the newly identified UCDs, along with their spectral classifications where the Q1 spectra quality allows for confident determination.

Key words. Stars: ultracool dwarfs, brown dwarfs — Methods: observational, data analysis — Techniques: photometric, spectroscopic

1. Introduction

Ultracool dwarfs (UCDs) are the lowest-mass, coldest, and faintest products of star formation (Kumar 1963; Hayashi & Nakano 1963). Kirkpatrick et al. (1997) defined them as ob-

* This paper is published on behalf of the Euclid Consortium

** e-mail: anjana.mohandas@univ-fcomte.fr

jects with spectral types M7 and later, having effective temperatures below 2700–2800 K (see Figure 4 in Ravinet et al. 2024), and masses $\lesssim 0.1 M_{\odot}$ (Dupuy & Liu 2017). They are fascinating objects in stellar astrophysics since they encompass both very low-mass stars that slowly fuse hydrogen (Burgasser 2004) and brown dwarfs (BDs), which have insufficient mass to sustain hydrogen fusion (below $\sim 0.075 M_{\odot}$ at solar metallicity, Burrows et al. 2001). With lifetimes exceeding the age of the Universe (Laughlin et al. 1997), they are present in all Galactic components, from young stellar associations to the halo, making them productive for Milky Way studies (Reid & Gizis 1997; Reyl   et al. 2021). Furthermore, they provide crucial insights into stellar-substellar formation, a process that is poorly understood and continues to be an active research focus (Maldonado et al. 2019; Vowell et al. 2025).

The unique nature of UCDs arises from distinct processes in their interior and surface layers that set them apart from typical stars (Fernandes et al. 2019; Chabrier et al. 2023). Their cool but complex atmospheres, with dust, condensation, and cloud coverage, are challenging to model (Morley et al. 2012; Burningham et al. 2021). Strong molecular absorption – due to H_2O , CO , NH_3 , and CH_4 – cause UCD spectra to deviate significantly from blackbody radiation, producing a pseudo-continuum (Manjavacas et al. 2019). Atmospheric properties depend on factors such as temperature, gravity, metallicity, cloud characteristics, and vertical mixing (Baraffe et al. 2015; Phillips et al. 2020), which are essential for spectral classification and energy distribution studies.

UCDs are classified into spectral types M, L, T, and Y, based on their spectral features. M dwarfs exhibit TiO and VO bands, which weaken in L dwarfs, where H_2O and CO absorption dominate. T dwarfs show characteristic CH_4 absorption in the near-infrared (NIR), which strengthens in Y dwarfs alongside the emergence of NH_3 absorption (Burgasser et al. 2006; Cushing et al. 2011). Objects of spectral type M7 to L4 include both stars and young BDs, while objects beyond L4 are more likely to be BDs (Dupuy & Liu 2017). As UCDs cool over time, they transition through later spectral types, meaning that objects of the same spectral type can have different masses and effective temperatures (Burrows et al. 1997; Burgasser 2004).

UCDs are also emerging as key targets for exoplanet detection, particularly through the transit method (Gillon et al. 2016, 2017; Delrez et al. 2018), since their small radii enhance the detectability of orbiting planets. The atmospheres of low-mass BDs, when they are bright enough for spectroscopic observation, are much easier to study than those of exoplanets, which are often obscured by the light of their host stars and there are many systems with directly imaged substellar companions.

UCDs constitute a significant fraction of the Milky Way’s stellar population, with estimates suggesting they represent at least 15% of star-like objects in the solar neighborhood (Bartlett et al. 2017). However, detection difficulties lead to statistical incompleteness; Bardalez Gagliuffi et al. (2019) estimate that only 69–80% of M7–L5 objects have been detected within 25 pc. Their faint luminosities and primarily NIR emission make UCDs challenging to observe, with most being too faint for *Gaia* and ground-based telescopes (Smart et al. 2017, 2019; Mace et al. 2013).

Euclid’s deep and wide surveys (Euclid Collaboration: Mellier et al. 2024; Euclid Collaboration: Cropper et al. 2024; Euclid Collaboration: Jahnke et al. 2024) will transform UCD studies, enabling the discovery of unprecedented numbers of objects. Simulations predict *Euclid* will detect nearly one million L dwarfs, 500 000 T dwarfs, and a few Y dwarfs (Solano et al.

2021). The resulting homogeneous sample will provide valuable insights into UCD demographics, enabling the identification of rare, extreme, faint, and nearby objects.

In searching for UCDs, one of the primary methods involves photometric searches across optical (e.g., Leggett et al. 2000; Chiu et al. 2006), the near-infrared (e.g., Kirkpatrick et al. 1999; Pinfield et al. 2008), and mid- to far-infrared wavelengths (Cushing et al. 2011; Kirkpatrick et al. 2011). The most numerous contaminants in these searches are distant galaxies and QSOs, while in QSO searches, UCDs emerge as the major contaminant (Ba  ados et al. 2016; Mortlock et al. 2009; Temple et al. 2021). The effective separation of these objects often requires additional spectroscopic observations, which *Euclid* can provide.

There are three papers exploring UCDs in the first *Euclid* Quick Data Release (Q1 Euclid Collaboration: Aussel et al. 2025).   erjal et al. (2025, in this special issue) focus on discovering UCDs using photometric selection. Dominguez-Tagle et al. (2025) analyse *Euclid* spectra to classify UCDs, determining their effective temperatures, ages, and radial velocities, and to search for new ones using spectral indices. In this paper, we use known objects to gain deeper insight into the contents of Q1 and its applications for UCD science. We search the *Euclid* Deep Field North (EDF-N) to identify new UCD candidates and assess our ability to distinguish them from QSOs using photometric methods.

The paper is structured as follows. Sect. 2 presents the sample from the EDF-N and a comparison sample of spectroscopically and photometrically identified UCDs. In Sect. 3, we determine the spectral types of the UCDs in the EDF-N sample using template fitting on their Q1 spectra. We discuss some of the difficulties of using the Q1 spectroscopy and match it to external comparison lists. In Sect. 4, examines the UCD distribution and predicted QSO locus in colour-colour planes. For new UCDs, we estimate their proper motions (PMs) and distances. We summarise our conclusions in Sect. 5. Appendix A provides the details of the electronic table containing the UCDs analysed in this study, including the newly discovered ones, while Appendix B investigates various *Euclid* fluxes to identify the most suitable choice for pointlike sources.

2. New UCD candidates and comparison sample

2.1. New UCD candidates in the EDF-N

As part of the process of searching for QSOs identified by the standard *Euclid* pipeline through $C III]$ and $Mg II$ emission lines, spectroscopic template fitting was used to identify other objects that share colour space with QSOs. This approach enabled a purely spectroscopic identification of UCDs and QSOs and allowed us to evaluate the pipeline’s ability to distinguish between them. This procedure was applied to the Q1 spectra (Euclid Collaboration: Le Brun et al. 2025; Euclid Collaboration: Copin et al. 2025) of objects in the EDF-N (22.9 deg² centred on RA = 17^h 58^m 55^s.9 and Dec = 66   1’ 4’’.7) and resulted in 202 UCD candidates, which were provided to the *Euclid* UCD working group for further investigation (Vincent Le Brun and Eduardo Ba  ados, private communication). In this paper, we analyse this sample of new UCDs.

2.2. Comparison sample of known UCDs found in Q1

As a comparison sample, we searched for known UCDs in Q1. We cross-matched the Q1 merged catalogue (hereafter Q1 MER, Euclid Collaboration: Romelli et al. 2025) available in the *Euclid*

Table 1. Selected UCDs with photometric and spectroscopic spectral types from the literature. The bracketing of the spectral type means it is based on photometry rather than spectroscopy. J_E is the *Euclid* AB magnitude based on the 2FWHM flux, J is a Vega magnitude in either the 2MASS or MKO photometric systems as defined by the reference.

Short name	<i>Euclid</i> Name	Simbad Name	J_E	J	SpT
J0332–2733	EUCL J033234.44–273333.9	WISEA J033234.35–273333.8	18.301	17.26 ¹	M9 ¹
J0352–4910	EUCL J035231.98–491058.8	WISEA J035231.80–491059.4	19.520	17.86 ¹	T7 ¹
J0359–4740	EUCL J035909.93–474057.4	WISEA J035909.75–474056.8	19.763	18.11 ¹	T7.5 ¹
J0402–4704	EUCL J040254.89–470440.2	WISEA J040254.85–470440.9	20.050	18.97 ¹	L4.5 ¹
J0403–4916	EUCL J040351.20–491603.5	CWISE J040351.12–491605.4	21.907	20.19 ²	(T7) ²
J0413–4750	EUCL J041358.31–475035.0	WISE J041358.14–475039.3	21.447	19.62 ²	T9 ³
J0416–4721	EUCL J041657.68–472115.9	WISE J041657.60–472115.0	19.964	18.42 ¹	(T2–T5) ⁴
J1745+6459	EUCL J174556.40+645937.1	WISE J174556.65+645933.8	19.967	19.00 ³	T7 ³
J1754+6712	EUCL J175410.42+671212.4	WISEA J175410.34+671212.0	17.487	16.13 ⁴	L1 ¹
J1757+6741	EUCL J175730.71+674136.5	2MASS J17573073+6741401	20.257	13.70 ⁴	M9 ¹
J1811+6658	EUCL J181125.15+665801.8	CWISE J181125.34+665806.4	22.073	21.61 ⁵	(T9) ⁵
J1819+6600	EUCL J181949.30+660059.1	2MASS J18194942+6600548	26.960	15.43 ⁴	(L2) ⁶

Photometric references : 1, [Khrantsov et al. \(2021\)](#); 2, [Leggett et al. \(2021\)](#); 3, [Mace et al. \(2013\)](#), 4, [Cutri et al. \(2003\)](#), 5, [Kirkpatrick et al. \(2024\)](#) Spectral type references 1: [Zhang et al. \(2024\)](#); 2, [Rothermich et al. \(2024\)](#); 3, [Mace et al. \(2013\)](#); 4, [Pinfield et al. \(2014\)](#); 5, [Kirkpatrick et al. \(2024\)](#); 6, [Sebastian et al. \(2021\)](#).

science archive¹ with a compilation of already known UCDs described below.

2.2.1. UCDs from DES+VHS+WISE

[Carnero Rosell et al. \(2019\)](#) presents extensive catalogues of candidate UCDs, including 11 745 photometrically classified objects near the stellar-substellar boundary and BDs, with spectral types ranging from L0 to T9, and 20 863 dwarfs with spectral types ranging from M6 to M9. These candidates have detections in common between the Dark Energy Survey (DES) Year-3 data ([Flaugher et al. 2015](#)), Vista Hemisphere Survey (VHS) DR3 data ([McMahon et al. 2013](#)), and Wide-field Infrared Survey Explorer (WISE, [Wright et al. 2010](#)). These catalogues cover 2400 deg² in the southern sky and combine photometric information from eight filters.

We searched for counterparts of DES objects in Q1 data within a radius of 5'' around the DES position. This often yields more than one match. To remove incorrect matches, we compared magnitudes in *Euclid* filters I_E and Y_E with I and Y magnitudes from DES, as well as J_E and H_E with J and H from VHS². We rejected all matches having a magnitude difference of > 1 mag in one or more of the four filter combinations. All *Euclid* magnitudes are obtained using the flux from aperture photometry of aperture size twice full width at half maximum (2FWHM), available in the *Euclid* MER catalogue, which is the most appropriate for point-like objects (see Sect. 4.1).

For objects passing this filtering, a figure of merit (FoM) is calculated as,

$$\text{FoM} = \sqrt{\sum_{M=I,Y,J,H} \left(\frac{\Delta M}{\sigma_M} \right)^2 + \sum \left(\frac{S}{\sigma_S} \right)^2} \quad (1)$$

¹ <https://eas.esac.esa.int/sas/>

² The zero points used for conversions between magnitudes and fluxes and for conversion between AB and Vega magnitude systems are taken from SVO Filter Profile Services ([Rodrigo et al. 2012](#)). Magnitude conversions between *Euclid* and observations from other surveys are carried out using the relations reported in appendix D of [Euclid Collaboration: Jahnke et al. \(2024\)](#).

where S is the separation between the DES and Q1 positions, and M represents the magnitude in the four photometric bands. The best crossmatch is selected as the pair that minimises the FoM value. We recovered 326 M7 to L6 dwarfs, consisting of 220 M dwarfs and 106 L dwarfs, as reliable matches of DES objects in Q1.

2.2.2. UCDs from the literature

We cross-matched the Q1 data set with the catalogue of known UCDs from [Smart et al. \(2019\)](#). This catalogue has been updated since publication to include all spectroscopically classified objects later than M9 published before 2024, as well as examples of earlier spectral types. The latest, unpublished version contains 8 435 spectroscopically and 3 821 photometrically classified UCDs spanning spectral types M7 to Y3, distributed across the sky. Our cross-match identified 12 objects of spectral types M9 to T9, classified spectroscopically and photometrically (hereafter LIT); these are listed in Table 1.

The initial match was performed by selecting the nearest Q1 entry within a 5'' radius of each UCD. When PMs were available, we updated the positions to epoch 2024.6, consistent with Q1 data. If PMs were unavailable, we used the original discovery position, which was often based on ground-based catalogues with epochs typically from the early 2000s. Multiple matches often occurred within a few arcseconds. The best magnitude match was not always the closest to the predicted position due to the UCD's PM. To resolve such cases, we applied the method described for the DES catalogue in Sect. 2.2.1 to identify the correct counterparts. Table 1 lists two matched objects, J1757+6741 and J1819+6600, which exhibit significant magnitude differences. These objects are saturated in *Euclid* observations, making their magnitudes unreliable. However, visual inspection confirmed the match and their observed spectra agree with their spectral classifications. When using magnitude differences as a secondary match criterion bright objects should be visually confirmed.

3. Spectral classification

In this section, we present the spectral standard fitting of UCD candidates with Q1 spectra to derive their spectral type. The data points that make up each Q1 spectrum are filtered to select high-quality and reliable measurements. We excluded measured points shortward of $1.22\ \mu\text{m}$ and redder than $1.88\ \mu\text{m}$ from our fitting range to avoid noise at the edges of the spectrum. Additionally, points with MASK parameter value of zero are selected to obtain superior quality measurements. The good-quality spectral points are then used to calculate the signal-to-noise ratio (S/N) of the spectra and are compared to the template spectrum to find the UCD spectral type along with an estimate of the χ^2 of the fit.

To determine the spectral types of the Q1 spectrum, we used a ‘classify by standard’ method within the SpeX Prism Library Analysis Toolkit (SPLAT, Burgasser & Splat Development Team 2017). For each Q1 spectrum being analysed, the SPLAT fitting routine performs a χ^2 minimisation with each of the possible spectral standards considered. The UCD standard spectra used in the fitting are obtained from Burgasser et al. (2006), Kirkpatrick et al. (2010), and Cushing et al. (2011).

3.1. Quality check on the comparison sample

Before applying spectral analysis and standard spectral fitting to the new UCD Q1 candidates, we first tested the method on our comparison sample as a validation step. A total of 109 spectra meet our quality criteria and are included in the comparison sample. The sample includes 104 objects with photometrically derived spectral types: 103 from the DES sample and one from the LIT sample. Additionally, five objects from the LIT sample have spectroscopically determined spectral types. The spectral types derived from Q1 spectra are consistent with their DES and LIT classifications, with a standard deviation of 1.86. This suggests an average difference of one to two spectral subtypes between Q1 and literature values.

Figure 1 presents the Q1 spectra of four LIT objects. Black points represent the observed spectrum, while blue points indicate data retained after quality filtering. Only the blue points are used for spectral standard fitting, as described in Sect. 3. The green lines represent the template spectrum corresponding to the previously published spectral classifications.

J0352–4910 (WISEA J035231.80–491059.4) is a T7 dwarf discovered by Zhang et al. (2024). The Q1 observations are of high quality, with only a few points removed by our quality filter. Our spectral fit yields the same classification as reported in the literature.

J1819+6600 (2MASS J18194942+6600548) has a photometrically derived spectral type of L2.2 from Sebastian et al. (2021). Our spectral fit also classifies it as an L2. This object is very bright ($J = 15.43$; Cutri et al. 2003), leading to saturation in the *Euclid* data and rendering the J_e magnitude unreliable. Several rejected data points deviate from the spectral template. Since this source is bright, it is also detected in *Gaia* DR3 (source ID 2257578507499901312) with a parallax of $(28.3 \pm 0.6\ \text{mas})$, consistent with an L2 classification. This result demonstrates that even with partial spectral data, a reliable classification can still be obtained, highlighting the importance of proper spectral filtering.

In contrast, the T9 dwarf J0413–4750 (WISE J041358.14–475039.3; Mace et al. 2013) exhibits a Q1 spectrum that deviates from all available spectral templates, despite minimal data rejection. We examined the *Euclid* images to determine whether the poor fit of the spectrum could be

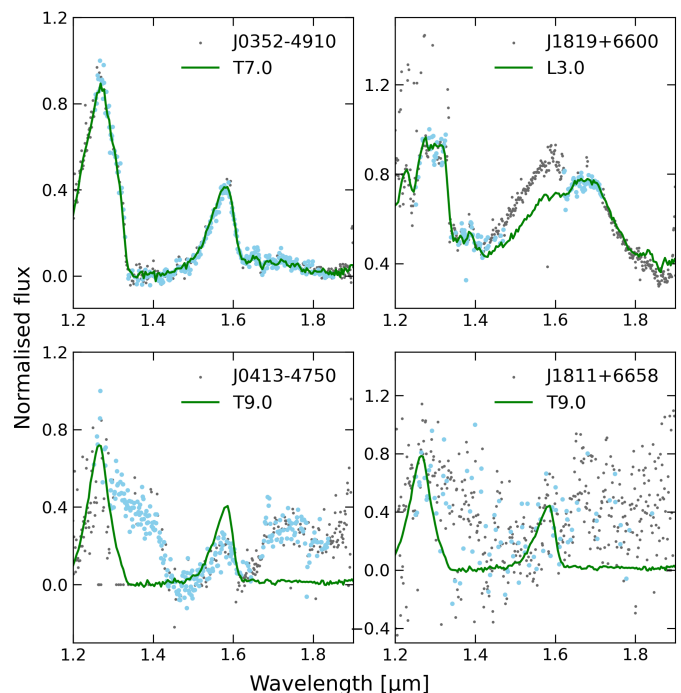


Fig. 1. Q1 spectra of four UCDs with published spectral classifications. The solid green line represents the template spectrum corresponding to the published spectral type. Grey points denote all measured data, while blue points indicate those retained after quality filtering.

attributed to detector artefacts or contamination from a nearby source. However, no conclusive explanation has been found for the mismatch between the observed spectrum and UCD templates.

The final example shown in Fig. 1 (bottom right) is J1811+6658 (CWISE J181125.34+665806.4), recently identified as a brown dwarf candidate within 20 pc by Kirkpatrick et al. (2024). In that study, the authors reported a parallax of (69.7 ± 6.8) mas and a proper motion exceeding $0.5''\text{yr}^{-1}$. Based on this distance, apparent magnitude, and colour, they classified J1811+6658 as a T9–Y1 dwarf. However, our spectral fitting procedure assigns it an L4 spectral type. In Fig. 2, we present a Keck MOSFIRE *J* band image of this object from 2021 alongside the *Euclid* image from 2024 with its predicted trajectory until 2034 (the anticipated end of an extended *Euclid* mission). At present, J1811+6658 overlaps with a background object and is assigned to the Q1 detection OBJECT_ID = 2728547962669671905. The incorrect spectral classification results from significant contamination by this background source. In future *Euclid* observations, as the brown dwarf moves further along its trajectory, it will become isolated, enabling an uncontaminated spectral measurement.

3.2. Spectral types of new candidates

Spectral analysis and SPLAT spectral standard fitting are applied to the sample of 202 UCD candidates. Among them, 33 have high-quality Q1 spectra that allow us to derive a confident spectral type. They are listed in Table 3.1. High-quality spectra representative of unique spectral types from M7 to T0, along with their best-fit SPLAT standard, are shown in Figure 3.

Some of the remaining objects have interesting spectra, but deviate from the UCD standard spectra. We describe two examples below. Figure 4 shows the Q1 spectrum of J1813+6557

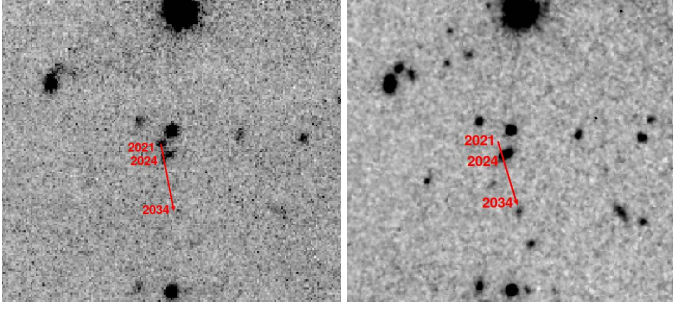


Fig. 2. *Left:* Keck MOSFIRE J (MKO) band image from 27 August 2021, showing J1811+6658 and its predicted positions in 2024 and 2034. *Right:* Q1 background-subtracted J_E image from 18 July 2024, with identical position markings.

Table 2. 33 new UCD candidates in EDFN with high-quality NISP spectrum. The spectral type (SpT) is derived from Q1 NISP spectra.

Short name	Euclid name (EUCL)	J_E	SpT
J1821+6653	J182133.43+665312.2	20.593	M7.0
J1808+6621	J180845.29+662118.7	19.971	M8.0
J1737+6621	J173729.32+662141.7	19.317	M8.0 ^{1,2}
J1802+6611	J180242.86+661100.3	19.167	M8.0
J1816+6540	J181650.97+654019.0	19.693	M8.0
J1730+6536	J173038.36+653630.0	19.582	M8.0
J1753+6600	J175339.09+660028.0	20.978	M9.0
J1801+6435	J180119.12+643547.0	20.060	M9.0
J1801+6832	J180120.11+683231.0	19.334	M9.0
J1812+6739	J181217.66+673947.4	19.549	L0.0
J1752+6811	J175224.29+681130.8	20.557	L0.0
J1752+6710	J175224.03+671045.1	19.802	L0.0 ^{1,2}
J1800+6604	J180005.51+660416.6	19.392	L0.0
J1755+6712	J175516.15+671214.6	18.166	L1.0
J1755+6322	J175557.68+632200.6	19.574	L1.0
J1749+6326	J174906.70+632637.3	19.273	L1.0
J1732+6547	J173225.69+654747.9	19.390	L1.0
J1744+6653	J174441.74+665349.4	19.076	L1.0
J1800+6719	J180046.67+671902.4	19.603	L1.0
J1806+6623	J180624.15+662345.2	19.902	L2.0 ^{1,2}
J1732+6555	J173222.86+655522.6	20.162	L2.0
J1745+6427	J174526.94+642725.0	19.867	L2.0 ^{1,2}
J1802+6517	J180247.62+651738.8	17.824	L3.0 ^{1,2}
J1801+6321	J180120.97+632100.2	21.084	L4.0
J1754+6551	J175418.85+655123.3	20.339	L4.0
J1744+6406	J174409.24+640638.8	17.763	L4.0
J1801+6708	J180153.19+670853.1	19.662	L5.0
J1801+6623	J180142.91+662327.5	20.961	L7.0
J1812+6616	J181201.84+661609.7	20.212	L7.0
J1746+6419	J174645.56+641933.6	20.609	L7.0
J1815+6456	J181528.44+645627.1	20.250	L7.0
J1807+6401	J180754.09+640141.4	19.078	L7.0
J1807+6642	J180744.18+664252.8	19.906	T0.0 ¹

1: also found by Dominguez-Tagle et al. (2025).

2: also found by Žerjal et al. (2025).

(OBJECT_ID = 2734840299659521922), which has 315 pixels meeting the quality cuts, with a mean S/N of 17.66. It displays spectral features different from those of a normal UCD template, including a narrow H band peak and a peculiar dip around 1.3 μm . Since the triangular-like shape of the H band is characteristic of young, low-gravity objects, we compare in Fig. 4 the spec-

trum of J1813+6557 with the spectrum of a very low-gravity L7 from ground-based observations (Bouy et al. 2022) and a very low-gravity L5 taken from the Cloud Atlas JWST UCD spectra archive (Manjavacas et al. 2019). We also plot the spectrum of a normal L5 dwarf from the Cloud Atlas JWST UCD spectra archive. Although the Q1 spectrum does not correspond exactly to any of these, it shows that the low-gravity spectrum have a depressed flux in the J band. The JWST spectra, not hampered by telluric absorption, also show a higher flux at 1.4 μm in the very-low gravity object.

Figure 5 displays the Q1 spectrum of object J1816+6432 (OBJECT_ID = 2741779784645475127), which has a high mean S/N of 102.06 with 180 pixels meeting the quality cuts. Its peak in the H band is similar to that of T dwarfs. However, half of it is filtered out after applying the selection criteria, and there are no signals in the J band. Nevertheless, it might be a good late-T-type candidate.

Further investigation of these objects is beyond the scope of this study. The rest of the sample has insufficient quality spectra to assign spectral types.

4. Colours, motions and distances

In total, we were able to retrieve spectral types from Q1 spectra for 142 UCDs, including the 33 new EDF-N UCDs. Table A provides the primary data used within this contribution. The spectra can be directly obtained from the *Euclid* science archive using their object_id.

4.1. Euclid colours

Euclid MER catalogues provide fluxes derived by various methods in each photometric band (Euclid Collaboration: Aussel et al. 2025). Fluxes from model-fitting photometry using Ser-sic models (Kümmel et al. 2022) and aperture photometry (A-PHOT, Merlin et al. 2019) are available for all the bands. A-PHOT offers four different fluxes, calculated within aperture diameters of $1\times\text{FWHM}$, $2\times\text{FWHM}$, $3\times\text{FWHM}$, and $4\times\text{FWHM}$. Flux calculated by Template fitting photometry (T-PHOT, Merlin et al. 2015) is available for NIR bands, while PSF-fitting photometry is provided for the VIS band.

To find the best choice of MER flux for point-like sources such as UCDs, we computed the deviation of the corresponding magnitudes from the published magnitude for the 103 selected DES objects. Figure B.1 shows the deviation of I_E and Y_E from DES I and Y in the top panels and the deviation of J_E and H_E from VHS J and H magnitude in the bottom panel. From the standard deviation of the distribution, denoted in the legend, A-PHOT in $2\times\text{FWHM}$ is the closest to DES/VHS magnitudes in Y , J , and H filter; we have therefore adopted this as our default flux to calculate magnitudes.

Figure 6 presents *Euclid* colour-colour diagrams for various filter combinations. The sample includes 142 UCDs with spectral types derived from their Q1 spectra. Given the low number of T dwarfs in the data set, we supplement the sample with 10 T dwarfs from Dominguez-Tagle et al. (2025), to uniformly examine the spectral subtype range. On average, the colour-colour diagrams exhibit a correlation between spectral type and colour. This trend was predicted by Sanghi et al. (2024) using synthetic *Euclid* colours of UCDs.

In each panel of Figure 6, we have included the predicted QSO tracks with redshifts from $z = 5$ to $z = 9$. The tracks, constructed using qsogen QSO modelling codes, are taken from

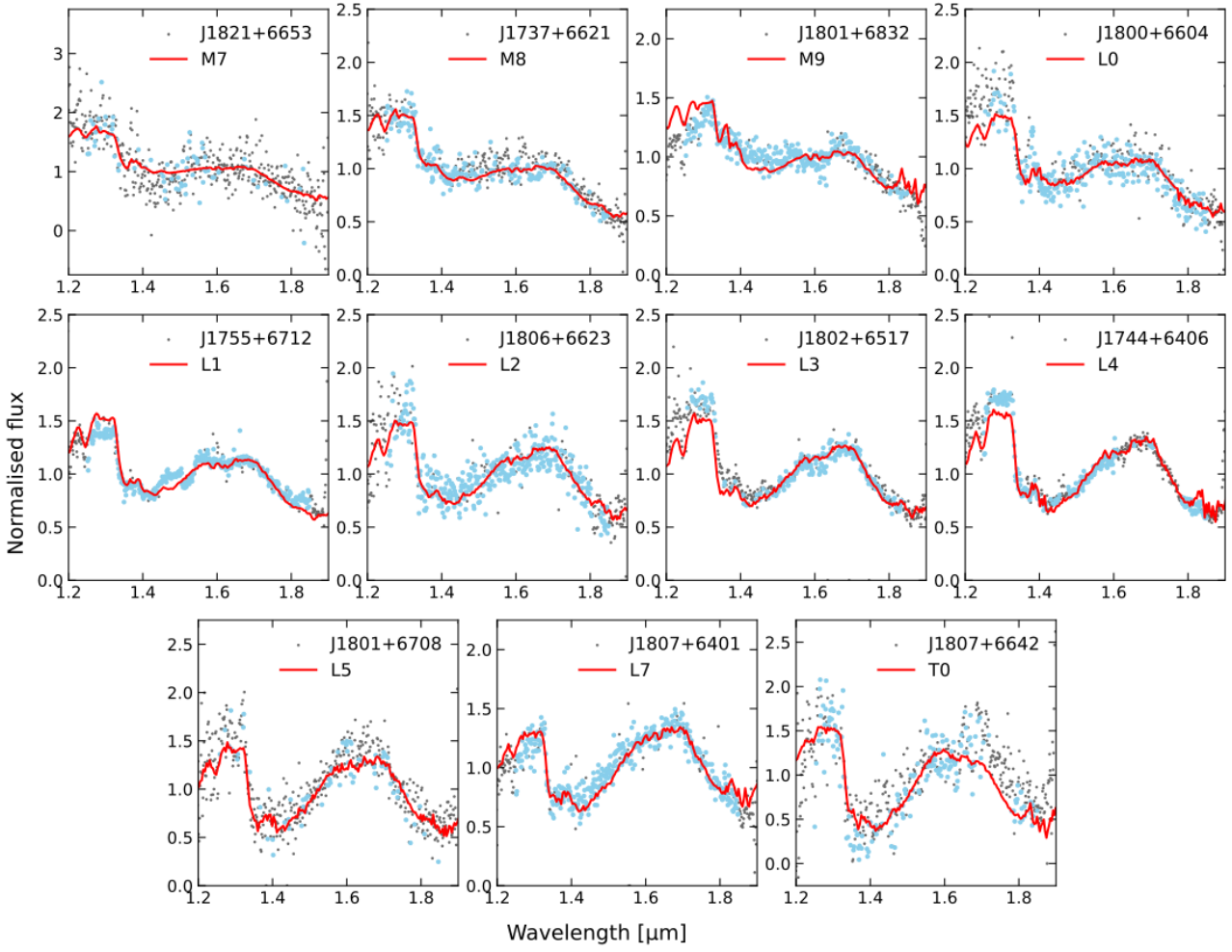


Fig. 3. The Q1 spectra of a subset of newly discovered UCDs in the EDF-N are shown. Black and blue points represent all data points and those selected after quality-based filtering, respectively. The standard spectra, corresponding to the determined spectral type, are shown in red.

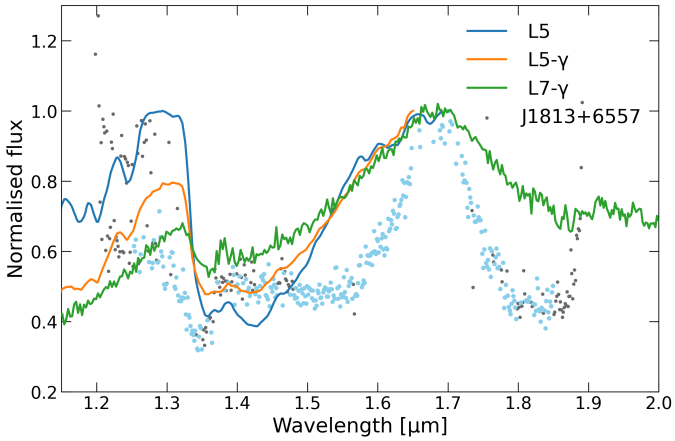


Fig. 4. Peculiar spectrum of J1813+6557, along with spectra of very low-gravity and a normal L5 from JWST and a very low-gravity L7 observed from the ground, for comparison (refer to Sect. 3.2). Spectra are normalised at 1.7 μm .

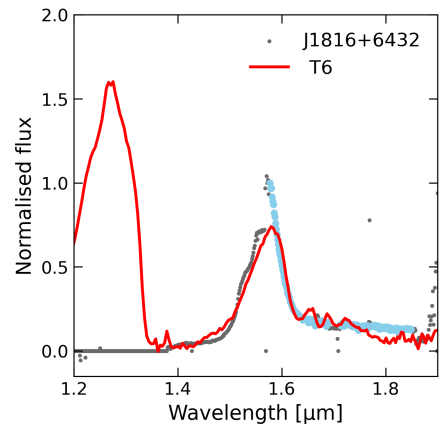


Fig. 5. The high S/N spectrum of J1816+6432, for which measurements in the J band are missing.

Temple et al. (2021). The default predictions of the QSO model are indicated in a white dashed line, and the redshift values are labelled. Dashed lines in light blue, dark blue, light red, dark red, light green, and dark green denote extremely weak-lined

QSOs, extremely strong-lined QSOs, dust extinction of $E(B-V) = 0.1$ and $E(B-V) = 0.2$ in the QSO rest frame, and extremely weak-lined QSOs with $E(B-V) = 0.1$ and strong-lined QSOs with $E(B-V) = 0.1$. These tracks are consistent with the predicted loci in other studies (Euclid Collaboration: Barnett et al. 2019; Tee et al. 2023), and show significant overlap with M and

Table 3. *Euclid* deep field observation start, length, and mean epoch.

Field	Start [yr]	Length [d]	Mean [yr]
EDF-N	2024.5439	2.192	2024.5469
EDF-F	2024.5965	1.166	2024.5981
EDF-S	2024.6806	2.654	2024.6842

L dwarfs in the colour space, suggesting that the separation of the two populations requires spectroscopic investigation in addition to photometric selections.

4.2. Proper motions

To calculate the PMs of objects in the three fields, we require a first-epoch observation covering the entire footprint of all three. The only survey that meets these criteria while detecting objects as faint as UCDs is the WISE survey. We use the AllWISE positions since they are based on observations taken over a short time frame, ensuring internally consistent positions at a single epoch (2010.5589). Table 3 lists the mean epochs of the three EDFs. Combined with AllWISE, it provides an epoch difference of approximately 14 years.

Euclid entries were matched to the AllWISE catalogue using a $10''$ radius, accommodating objects with PMs up to $0.7''\text{yr}^{-1}$. Since Q1 lacks a photometric band close to the AllWISE bands, magnitude differences could not be used as a selection criterion. Consequently, the high search radius resulted in numerous mismatches. For the 33 new objects, we manually verified the AllWISE match to ensure correct identification.

AllWISE positions were determined using a combination of the Fourth United States Naval Observatory (USNO) CCD Astrograph Catalog (UCAC4, Zacharias et al. 2013) and 2MASS³, whereas *Euclid* uses the *Gaia* DR3 catalogue. This introduces potential systematic differences between the two reference frames. To mitigate this, we adjusted *Gaia* DR3 matches to AllWISE objects to epoch 2010.5589 and applied the Infinity Overlapping Circles (Bucciarelli et al. 1993) method to align them with the *Gaia* reference frame. A comparison of the derived PMs to objects with *Gaia* PMs indicated that the derived values and their errors are consistent.

Figure 7 presents reduced proper motion (RPM) diagrams for our comparison. New objects are represented as diamonds, colour-coded by spectral type, while sources common to both AllWISE and Q1 appear as black dots. Different black cloud regions correspond to halo and disc Galactic populations. The left panel ($J_E - H_E$ RPM diagram) shows a clear separation between these populations. The right panel, which includes visible and NIR bands (I_E and Y_E RPM diagrams), demonstrates how these colours help isolate UCDs from halo and disc objects.

4.3. Spectroscopic Distances

For all UCDs in the combined catalogue, we calculated spectroscopic distances using the spectral types derived in this work and *Euclid* magnitudes, following the empirical relation from Sanghi et al. (2024). We compared these distances to both trigonometric measurements from *Gaia* and photometric estimates derived from transformed magnitudes using absolute magnitude calibrations in the literature. In both cases, our spectroscopic distances

were found to be consistent. Figure 8 presents spectral type versus spectroscopic distance. As expected, late L and T dwarfs are located within 100 pc, while late M dwarfs extend to distances of 500–600 pc.

4.4. Possible companions

Using the positions, PMs, and spectroscopic distances, we searched *Gaia* DR3 for possible companions to the newly detected UCDs. Spectroscopic “parallaxes” (ϖ_{SpT}) in mas were computed as 1000 divided by the derived spectroscopic distances. The associated uncertainties were set equal to the relative errors in the spectroscopic distances. Due to the large uncertainties in our parallaxes, we limited our search to objects with $\varpi_{\text{SpT}} > 8$ mas. Our selection criteria for companions were a slight variation of those used in Smart et al. (2019). In summary:

- the projected separation on the sky must be less than 200 000 au at the distance of the *Euclid* UCD,
- the parallaxes must agree within $3 \times \left(\sqrt{\sigma_{\varpi_{\text{SpT}}}^2 + \sigma_{\varpi}^2} \right)$,
- and the proper motion modulus and direction must be consistent within 20%.

Two of the new EDF-N UCDs, J1755+6712 and J1815+6456, have candidate companions based on this criterion, as listed in Table 4. J1755+6712 has two *Gaia* DR3 objects that are both considered to have good astrometry but have probable distances that differ significantly: 97 pc and 116 pc for *Gaia* DR3 1633630913145871360 and 1633663516243870464, respectively (Gaia Collaboration et al. 2021). The large uncertainty in the *Euclid* UCD distance means that this is not a strong constraint, leading to possible false positives. Indeed, the two candidate companions, with more precise *Gaia* parameters, would not meet the selection criteria. This may also be the case for the companion to J1815+6456 given the large nominal distance differences. Since these UCDs are deep-field objects visible in a single pass, the multiple passes planned for the EDFs will allow the calculation of parallaxes, significantly reducing the largest source of uncertainty.

5. Conclusions

This work leverages the new Q1 spectra to identify UCDs based solely on their spectral features, without prior filtering on morphological parameters. We assess the capability of this method by applying it to known UCDs in Q1 with ground-based spectra. NIR colours provide an effective means of classifying UCDs, with high-redshift QSOs being the primary point-source contaminants. UCDs exhibit significantly redder VIS–NIR colours compared to QSOs (Euclid Collaboration: Barnett et al. 2019, see, e.g., their Fig. 1) and may be undetectable in the optical. However, at the current stage of our analysis, it remains unclear whether UCDs can be reliably distinguished from QSOs using Q1 photometry alone. For the brighter objects, *Euclid* spectra are sufficient to differentiate between QSOs and UCDs.

As discussed in Sect. 3.1, studying faint, fast-moving objects presents significant challenges. In many ways, *Euclid* is a victim of its own success. Its exceptionally faint magnitude limit results in a confusion-limited sky, complicating cross-matching and leading to significant spectral overlap. As we continue analysing *Euclid* data, new techniques will be developed to address these challenges and unlock the full potential of the mission. With the next *Euclid* observation runs, we expect to have better-quality

³ https://wise2.ipac.caltech.edu/docs/release/allwise/expsup/sec2_5.html

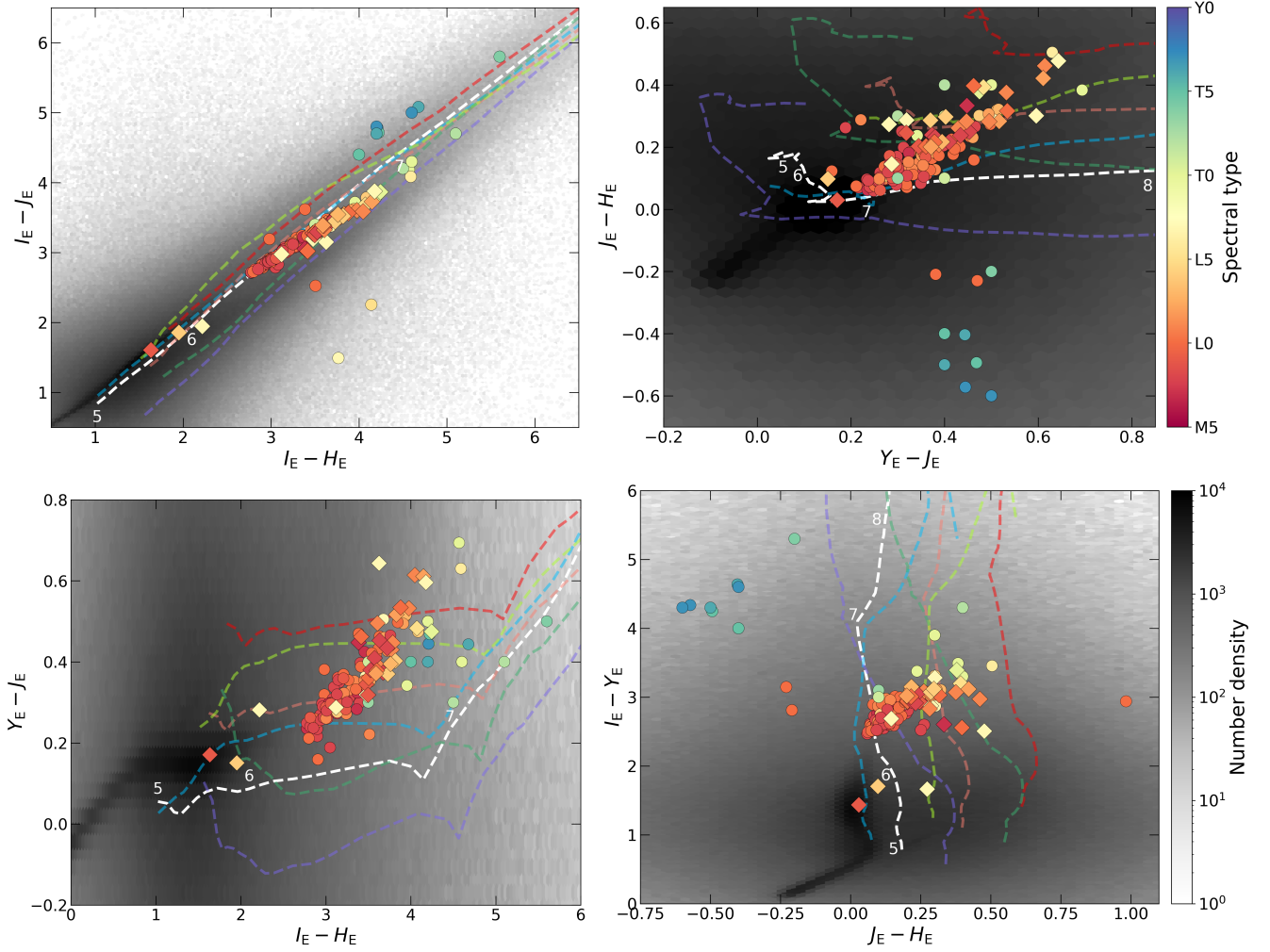


Fig. 6. 142 UCDs analysed in this study, of which 33 are newly identified with *Euclid*, displayed in various colour-colour diagrams, with only those having good quality spectrum and confident spectral typing included. Dots represent previously known UCDs with good-quality Q1 spectra. Diamonds represent new UCDs studied in this work with reliable spectral typing. They are colour-coded according to the spectral type assigned in this paper, which is displayed in the colour scale. Grey points are all Q1 objects with `point_like_probab` ≥ 0.8 with a shade that represents the number density as indicated in the scale. The dashed lines of different colours denote the expected position for typical QSOs with redshift from $z = 5$ to $z = 9$; White for default QSO position. Light and dark blue denote extremely weak and extremely strong lined QSO. Light and dark red denote $E(B-V)=0.1$ and 0.2 , in QSO rest frame. Light and dark green denote extremely weak and strong lined QSO with $E(B-V)=0.1$.

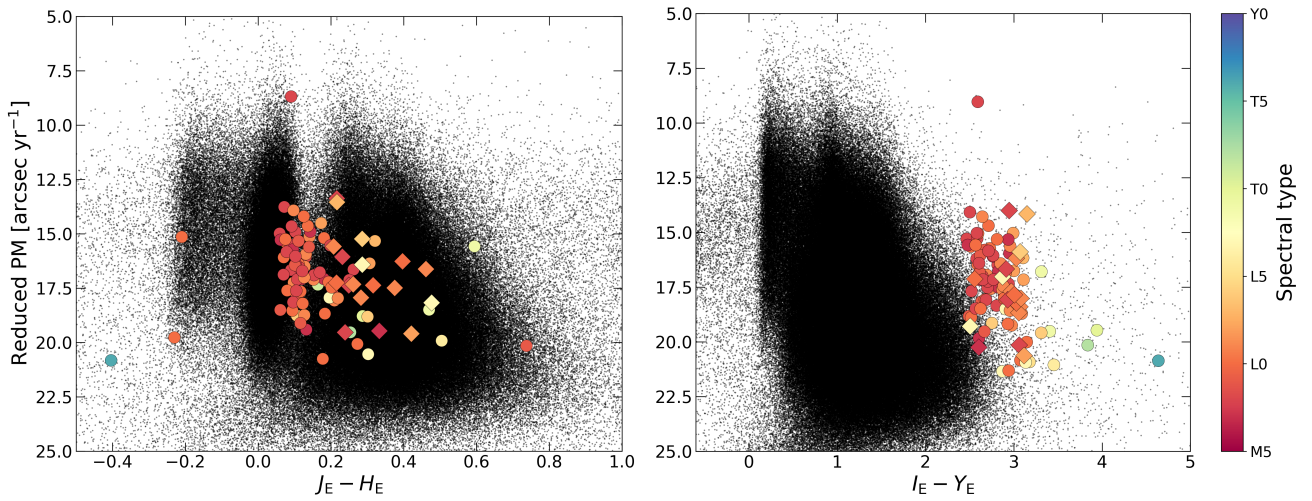


Fig. 7. Reduced proper motion diagrams for 142 UCDs, including 33 newly identified objects with reliable spectral typing. Newly identified UCDs are represented by diamonds, while known UCDs are shown as dots, colour-coded according to their assigned spectral type. Dark background points represent sources common to both AllWISE and Q1.

Table 4. Candidate companions to two new EDF-N UCDs. ϖ_{SpT} is the spectroscopic parallax, and ϖ is the *Gaia* parallax. S represents the projected on-sky separation in pc, assuming the UCD distance.

Short name	ϖ_{SpT} [mas]	μ_{α} [mas yr ⁻¹]	μ_{δ} [mas yr ⁻¹]	Gaia source_id candidate companion	S [kau]	ϖ [mas]	μ_{α} [mas yr ⁻¹]	μ_{δ} [mas yr ⁻¹]
J1755+6712	8.8±0.7	-54.3±8.9	68.2±9.0	1633630913145871360	14.44	10.29±0.06	-14.68±0.07	82.69±0.09
J1755+6712	8.8±0.7	-54.3±8.9	68.2±9.0	1633663516243870464	8.25	8.61±0.16	-37.90±0.19	68.47±0.20
J1815+6456	9.2±0.6	19.2±19.8	-3.7±18.9	2161277987739082880	16.50	5.49±1.33	19.25±1.40	6.02±1.59

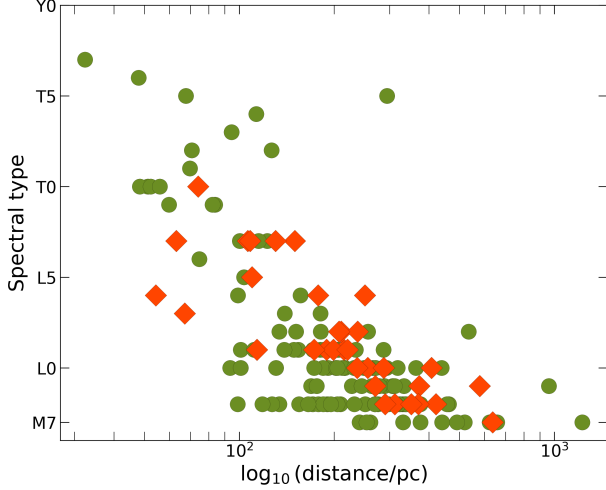


Fig. 8. Spectral type versus spectroscopic distance plot for newly identified and known UCDs. Newly identified UCDs are represented by red diamonds, while previously known UCDs are shown as green dots.

spectra for EDF-N objects and will be able to address the saturation and background contamination mentioned.

In this release, Q1 provides over 4 million spectra and 200 million photometric observations. In Žerjal et al. (2025), they identify over 5000 UCDs photometrically and estimate that *Euclid* will eventually observe more than 1.5 million.

The next *Euclid* data release, Data Release 1 (DR1), is scheduled for late 2026 and will cover approximately 1900 deg². It will include two compact regions in the northern sky and three compact regions in the southern sky, expanding the sky coverage by a factor of about 36 compared to Q1, while reaching progressively greater depths in the northern and southern deep fields. We anticipate significantly expanding the UCD sample, creating a large and homogeneous data set. This will enable unprecedented statistical analysis of various Milky Way populations, including its oldest members, and enhance our understanding of substellar formation history in the early Universe.

Acknowledgements. We would like to thank Dr. Matthew J. Temple for his help in constructing the QSO tracks and Davy Kirkpatrick/Federico Marocco for providing Keck MOSFIRE images. The Euclid Consortium acknowledges the European Space Agency and a number of agencies and institutes that have supported the development of *Euclid*, in particular the Agenzia Spaziale Italiana, the Austrian Forschungsförderungsgesellschaft funded through BMK, the Belgian Science Policy, the Canadian Euclid Consortium, the Deutsches Zentrum für Luft- und Raumfahrt, the DTU Space and the Niels Bohr Institute in Denmark, the French Centre National d'Études Spatiales, the Fundação para a Ciência e a Tecnologia, the Hungarian Academy of Sciences, the Ministerio de Ciencia, Innovación y Universidades, the National Aeronautics and Space Administration, the National Astronomical Observatory of Japan, the Nederlandse Onderzoeksschool Voor Astronomie, the Norwegian Space Agency, the Research Council of Finland, the Romanian Space Agency, the State Secretariat for Education, Research, and Innovation (SERI) at the Swiss Space Office (SSO), and the United Kingdom Space Agency. A complete and detailed list is available on the *Euclid* web site (www.euclid-ec.org). This work has made use of the *Euclid* Quick Re-

lease Q1 data from the *Euclid* mission of the European Space Agency (ESA), 2025, <https://doi.org/10.57780/esa-2853f3b>. *Euclid* Quick Release Q1 (2025) Based on data from UNIONS, a scientific collaboration using three Hawaii-based telescopes: CFHT, Pan-STARRS, and Subaru www.skysurvey.cc. Based on data from the Dark Energy Camera (DECam) on the Blanco 4-m Telescope at CTIO in Chile <https://www.darkenergysurvey.org>. This work uses results from the ESA mission *Gaia*, whose data are being processed by the Gaia Data Processing and Analysis Consortium <https://www.cosmos.esa.int/gaia>. Funding for CDT, ELM, MŽ, and JYZ was provided by the European Union (ERC Advanced Grant, SUBSTELLAR, project number 101054354) NL acknowledges support from the Agencia Estatal de Investigación del Ministerio de Ciencia e Innovación (AEI-MCINN) under grant PID2022-137241NB-C41. T. Dupuy acknowledges support from UKRI STFC AGP grant ST/W001209/1. For the purpose of open access, the author has applied a Creative Commons Attribution (CC-BY) licence to any Author Accepted Manuscript version arising from this submission.

References

- Bañados, E., Venemans, B. P., Decarli, R., et al. 2016, *ApJS*, 227, 11
Baraffe, I., Homeier, D., Allard, F., & Chabrier, G. 2015, *A&A*, 577, A42
Bardalez Gagliuffi, D. C., Burgasser, A. J., Schmidt, S. J., et al. 2019, *ApJ*, 883, 205
Bartlett, J. L., Lurie, J. C., Riedel, A., et al. 2017, *AJ*, 154, 151
Bouy, H., Tamura, M., Barrado, D., et al. 2022, *A&A*, 664, A111
Bucciarelli, B., Taff, L. G., & Lattanzi, M. G. 1993, *Journal of Statistical Computation and Simulation*, 48, 29
Burgasser, A. J. 2004, *ApJS*, 155, 191
Burgasser, A. J., Geballe, T. R., Leggett, S. K., Kirkpatrick, J. D., & Golimowski, D. A. 2006, *ApJ*, 637, 1067
Burgasser, A. J. & Splat Development Team. 2017, in *Astronomical Society of India Conference Series*, Vol. 14, *Astronomical Society of India Conference Series*, 7–12
Birmingham, B., Faherty, J. K., Gonzales, E. C., et al. 2021, *MNRAS*, 506, 1944
Burrows, A., Hubbard, W. B., Lunine, J. I., & Liebert, J. 2001, *Reviews of Modern Physics*, 73, 719
Burrows, A., Marley, M., Hubbard, W. B., et al. 1997, *ApJ*, 491, 856
Carnero Rosell, A., Santiago, B., dal Ponte, M., et al. 2019, *MNRAS*, 489, 5301
Chabrier, G., Baraffe, I., Phillips, M., & Debras, F. 2023, *A&A*, 671, A119
Chiu, K., Fan, X., Leggett, S. K., et al. 2006, *AJ*, 131, 2722
Cushing, M. C., Kirkpatrick, J. D., Gelino, C. R., et al. 2011, *ApJ*, 743, 50
Cutri, R. M., Skrutskie, M. F., van Dyk, S., et al. 2003, *VizieR Online Data Catalog: 2MASS All-Sky Catalog of Point Sources (Cutri+ 2003)*, *VizieR On-line Data Catalog: II/246*. Originally published in: University of Massachusetts and Infrared Processing and Analysis Center, (IPAC/California Institute of Technology) (2003)
Delrez, L., Gillon, M., Queloz, D., et al. 2018, in *Society of Photo-Optical Instrumentation Engineers (SPIE) Conference Series*, Vol. 10700, *Ground-based and Airborne Telescopes VII*, ed. H. K. Marshall & J. Spyromilio, 1070011
Dominguez-Tagle, C., Žerjal, M., Sedighi, N., et al. 2025, submitted to *ApJ*
Dupuy, T. J. & Liu, M. C. 2017, *ApJS*, 231, 15
Euclid Collaboration: Aussel, H., Tereno, I., Schirmer, M., et al. 2025, *A&A*, submitted, arXiv:2503.15302
Euclid Collaboration: Barnett, R., Warren, S. J., Mortlock, D. J., et al. 2019, *A&A*, 631, A85
Euclid Collaboration: Copin, Y., Fumana, M., Mancini, C., et al. 2025, *A&A*, submitted, arXiv:2503.15307
Euclid Collaboration: Cropper, M., Al Bahlawan, A., Amiaux, J., et al. 2024, *A&A*, accepted, arXiv:2405.13492
Euclid Collaboration: Jahnke, K., Gillard, W., Schirmer, M., et al. 2024, *A&A*, accepted, arXiv:2405.13493
Euclid Collaboration: Le Brun, V., Bethermin, M., Moresco, M., et al. 2025, *A&A*, submitted, arXiv:2503.15308

- Euclid Collaboration: Mellier, Y., Abdurro'uf, Acevedo Barroso, J., et al. 2024, A&A, accepted, arXiv:2405.13491
- Euclid Collaboration: Romelli, E., Kümmel, M., Dole, H., et al. 2025, A&A, submitted, arXiv:2503.15305
- Euclid Quick Release Q1. 2025, <https://doi.org/10.57780/esa-2853f3b>
- Fernandes, C. S., Van Grootel, V., Salmon, S. J. A. J., et al. 2019, ApJ, 879, 94
- Flaugher, B., Diehl, H. T., Vonscheid, K., et al. 2015, AJ, 150, 150
- Gaia Collaboration, Smart, R. L., Sarro, L. M., et al. 2021, A&A, 649, A6
- Gillon, M., Jehin, E., Lederer, S. M., et al. 2016, Nature, 533, 221
- Gillon, M., Triaud, A. H. M. J., Demory, B.-O., et al. 2017, Nature, 542, 456
- Hayashi, C. & Nakano, T. 1963, Progress of Theoretical Physics, 30, 460
- Khramtsov, V., Spiniello, C., Agnello, A., & Sergeyev, A. 2021, A&A, 651, A69
- Kirkpatrick, J. D., Cushing, M. C., Gelino, C. R., et al. 2011, ApJS, 197, 19
- Kirkpatrick, J. D., Henry, T. J., & Irwin, M. J. 1997, AJ, 113, 1421
- Kirkpatrick, J. D., Looper, D. L., Burgasser, A. J., et al. 2010, ApJS, 190, 100
- Kirkpatrick, J. D., Marocco, F., Gelino, C. R., et al. 2024, ApJS, 271, 55
- Kirkpatrick, J. D., Reid, I. N., Liebert, J., et al. 1999, ApJ, 519, 802
- Kumar, S. S. 1963, ApJ, 137, 1121
- Kümmel, M., Álvarez-Ayllón, A., Bertin, E., et al. 2022, arXiv e-prints, arXiv:2212.02428
- Laughlin, G., Bodenheimer, P., & Adams, F. C. 1997, ApJ, 482, 420
- Leggett, S. K., Geballe, T. R., Fan, X., et al. 2000, ApJ, 536, L35
- Leggett, S. K., Tremblin, P., Phillips, M. W., et al. 2021, ApJ, 918, 11
- Mace, G. N., Kirkpatrick, J. D., Cushing, M. C., et al. 2013, ApJS, 205, 6
- Maldonado, J., Villaver, E., Eiroa, C., & Micela, G. 2019, A&A, 624, A94
- Manjavacas, E., Apai, D., Zhou, Y., et al. 2019, AJ, 157, 101
- McMahon, R. G., Banerji, M., Gonzalez, E., et al. 2013, The Messenger, 154, 35
- Merlin, E., Fontana, A., Ferguson, H. C., et al. 2015, A&A, 582, A15
- Merlin, E., Pilo, S., Fontana, A., et al. 2019, A&A, 622, A169
- Morley, C. V., Fortney, J. J., Marley, M. S., et al. 2012, ApJ, 756, 172
- Mortlock, D. J., Patel, M., Warren, S. J., et al. 2009, A&A, 505, 97
- Phillips, M. W., Tremblin, P., Baraffe, I., et al. 2020, A&A, 637, A38
- Pinfield, D. J., Burningham, B., Tamura, M., et al. 2008, MNRAS, 390, 304
- Pinfield, D. J., Gomes, J., Day-Jones, A. C., et al. 2014, MNRAS, 437, 1009
- Ravinet, T., Reylé, C., Lagarde, N., et al. 2024, A&A, 685, A6
- Reid, I. N. & Gizis, J. E. 1997, AJ, 113, 2246
- Reylé, C., Jardine, K., Fouqué, P., et al. 2021, A&A, 650, A201
- Rodrigo, C., Solano, E., & Bayo, A. 2012, SVO Filter Profile Service Version 1.0, IVOA Working Draft 15 October 2012
- Rothermich, A., Faherty, J. K., Bardalez-Gagliuffi, D., et al. 2024, AJ, 167, 253
- Sanghi, A., Liu, M. C., Dupuy, T. J., et al. 2024, Research Notes of the American Astronomical Society, 8, 137
- Sebastian, D., Gillon, M., Ducrot, E., et al. 2021, A&A, 645, A100
- Smart, R. L., Marocco, F., Caballero, J. A., et al. 2017, MNRAS, 469, 401
- Smart, R. L., Marocco, F., Sarro, L. M., et al. 2019, MNRAS, 485, 4423
- Solano, E., Gálvez-Ortiz, M. C., Martín, E. L., et al. 2021, MNRAS, 501, 281
- Tee, W. L., Fan, X., Wang, F., et al. 2023, ApJ, 956, 52
- Temple, M. J., Hewett, P. C., & Banerji, M. 2021, MNRAS, 508, 737
- Vowell, N., Rodriguez, J. E., Latham, D. W., et al. 2025, arXiv e-prints, arXiv:2501.09795
- Žerjal, M., Dominguez-Tagle, C., Sedighi, N., et al. 2025, A&A, in preparation
- Wright, E. L., Eisenhardt, P. R. M., Mainzer, A. K., et al. 2010, AJ, 140, 1868
- Zacharias, N., Finch, C. T., Girard, T. M., et al. 2013, AJ, 145, 44
- Zhang, J. Y., Lodieu, N., & Martín, E. L. 2024, A&A, 686, A171
- ¹⁰ Centro de Astrobiología (CAB), CSIC-INTA, ESAC Campus, Camino Bajo del Castillo s/n, 28692 Villanueva de la Cañada, Madrid, Spain
- ¹¹ Institute for Astronomy, University of Edinburgh, Royal Observatory, Blackford Hill, Edinburgh EH9 3HJ, UK
- ¹² European Southern Observatory, Karl-Schwarzschild-Str. 2, 85748 Garching, Germany
- ¹³ Instituto de Astrofísica de Canarias, Vía Láctea, 38205 La Laguna, Tenerife, Spain
- ¹⁴ Universidad de La Laguna, Departamento de Astrofísica, 38206 La Laguna, Tenerife, Spain
- ¹⁵ Instituto de Astrofísica de Canarias (IAC); Departamento de Astrofísica, Universidad de La Laguna (ULL), 38200, La Laguna, Tenerife, Spain
- ¹⁶ Consejo Superior de Investigaciones Científicas, Calle Serrano 117, 28006 Madrid, Spain
- ¹⁷ Université Paris-Saclay, CNRS, Institut d'astrophysique spatiale, 91405, Orsay, France
- ¹⁸ ESAC/ESA, Camino Bajo del Castillo, s/n., Urb. Villafranca del Castillo, 28692 Villanueva de la Cañada, Madrid, Spain
- ¹⁹ School of Mathematics and Physics, University of Surrey, Guildford, Surrey, GU2 7XH, UK
- ²⁰ INAF-Osservatorio Astronomico di Brera, Via Brera 28, 20122 Milano, Italy
- ²¹ INAF-Osservatorio di Astrofisica e Scienza dello Spazio di Bologna, Via Piero Gobetti 93/3, 40129 Bologna, Italy
- ²² IFPU, Institute for Fundamental Physics of the Universe, via Beirut 2, 34151 Trieste, Italy
- ²³ INAF-Osservatorio Astronomico di Trieste, Via G. B. Tiepolo 11, 34143 Trieste, Italy
- ²⁴ INFN, Sezione di Trieste, Via Valerio 2, 34127 Trieste TS, Italy
- ²⁵ SISSA, International School for Advanced Studies, Via Bonomea 265, 34136 Trieste TS, Italy
- ²⁶ Dipartimento di Fisica e Astronomia, Università di Bologna, Via Gobetti 93/2, 40129 Bologna, Italy
- ²⁷ INFN-Sezione di Bologna, Viale Berti Pichat 6/2, 40127 Bologna, Italy
- ²⁸ INAF-Osservatorio Astronomico di Padova, Via dell'Osservatorio 5, 35122 Padova, Italy
- ²⁹ Space Science Data Center, Italian Space Agency, via del Politecnico snc, 00133 Roma, Italy
- ³⁰ Dipartimento di Fisica, Università di Genova, Via Dodecaneso 33, 16146, Genova, Italy
- ³¹ INFN-Sezione di Genova, Via Dodecaneso 33, 16146, Genova, Italy
- ³² Department of Physics "E. Pancini", University Federico II, Via Cinthia 6, 80126, Napoli, Italy
- ³³ INAF-Osservatorio Astronomico di Capodimonte, Via Moirariello 16, 80131 Napoli, Italy
- ³⁴ Instituto de Astrofísica e Ciências do Espaço, Universidade do Porto, CAUP, Rua das Estrelas, PT4150-762 Porto, Portugal
- ³⁵ Faculdade de Ciências da Universidade do Porto, Rua do Campo de Alegre, 4150-007 Porto, Portugal
- ³⁶ Dipartimento di Fisica, Università degli Studi di Torino, Via P. Giuria 1, 10125 Torino, Italy
- ³⁷ INFN-Sezione di Torino, Via P. Giuria 1, 10125 Torino, Italy
- ³⁸ European Space Agency/ESTEC, Keplerlaan 1, 2201 AZ Noordwijk, The Netherlands
- ³⁹ Institute Lorentz, Leiden University, Niels Bohrweg 2, 2333 CA Leiden, The Netherlands
- ⁴⁰ Leiden Observatory, Leiden University, Einsteinweg 55, 2333 CC Leiden, The Netherlands
- ⁴¹ INAF-IASF Milano, Via Alfonso Corti 12, 20133 Milano, Italy
- ⁴² Centro de Investigaciones Energéticas, Medioambientales y Tecnológicas (CIEMAT), Avenida Complutense 40, 28040 Madrid, Spain
- ⁴³ Port d'Informació Científica, Campus UAB, C. Albareda s/n, 08193 Bellaterra (Barcelona), Spain
- ⁴⁴ Institute for Theoretical Particle Physics and Cosmology (TTK), RWTH Aachen University, 52056 Aachen, Germany

- 45 INAF-Osservatorio Astronomico di Roma, Via Frascati 33, 00078 Monteporzio Catone, Italy
- 46 INFN section of Naples, Via Cinthia 6, 80126, Napoli, Italy
- 47 Institute for Astronomy, University of Hawaii, 2680 Woodlawn Drive, Honolulu, HI 96822, USA
- 48 Dipartimento di Fisica e Astronomia "Augusto Righi" - Alma Mater Studiorum Università di Bologna, Viale Berti Pichat 6/2, 40127 Bologna, Italy
- 49 Jodrell Bank Centre for Astrophysics, Department of Physics and Astronomy, University of Manchester, Oxford Road, Manchester M13 9PL, UK
- 50 European Space Agency/ESRIN, Largo Galileo Galilei 1, 00044 Frascati, Roma, Italy
- 51 Université Claude Bernard Lyon 1, CNRS/IN2P3, IP2I Lyon, UMR 5822, Villeurbanne, F-69100, France
- 52 Institut de Ciències del Cosmos (ICCUB), Universitat de Barcelona (IEEC-UB), Martí i Franquès 1, 08028 Barcelona, Spain
- 53 Institució Catalana de Recerca i Estudis Avançats (ICREA), Pas-seig de Luís Companys 23, 08010 Barcelona, Spain
- 54 UCB Lyon 1, CNRS/IN2P3, IUF, IP2I Lyon, 4 rue Enrico Fermi, 69622 Villeurbanne, France
- 55 Mullard Space Science Laboratory, University College London, Holmbury St Mary, Dorking, Surrey RH5 6NT, UK
- 56 Departamento de Física, Faculdade de Ciências, Universidade de Lisboa, Edifício C8, Campo Grande, PT1749-016 Lisboa, Portugal
- 57 Instituto de Astrofísica e Ciências do Espaço, Faculdade de Ciências, Universidade de Lisboa, Campo Grande, 1749-016 Lisboa, Portugal
- 58 Department of Astronomy, University of Geneva, ch. d'Ecogia 16, 1290 Versoix, Switzerland
- 59 INFN-Padova, Via Marzolo 8, 35131 Padova, Italy
- 60 Aix-Marseille Université, CNRS/IN2P3, CPPM, Marseille, France
- 61 INAF-Istituto di Astrofisica e Planetologia Spaziali, via del Fosso del Cavaliere, 100, 00100 Roma, Italy
- 62 School of Physics, HH Wills Physics Laboratory, University of Bristol, Tyndall Avenue, Bristol, BS8 1TL, UK
- 63 Universitäts-Sternwarte München, Fakultät für Physik, Ludwig-Maximilians-Universität München, Scheinerstrasse 1, 81679 München, Germany
- 64 Max Planck Institute for Extraterrestrial Physics, Giessenbachstr. 1, 85748 Garching, Germany
- 65 Institute of Theoretical Astrophysics, University of Oslo, P.O. Box 1029 Blindern, 0315 Oslo, Norway
- 66 Jet Propulsion Laboratory, California Institute of Technology, 4800 Oak Grove Drive, Pasadena, CA, 91109, USA
- 67 Department of Physics, Lancaster University, Lancaster, LA1 4YB, UK
- 68 Felix Hormuth Engineering, Goethestr. 17, 69181 Leimen, Germany
- 69 Technical University of Denmark, Elektrovej 327, 2800 Kgs. Lyngby, Denmark
- 70 Cosmic Dawn Center (DAWN), Denmark
- 71 NASA Goddard Space Flight Center, Greenbelt, MD 20771, USA
- 72 Department of Physics and Helsinki Institute of Physics, Gustaf Hållströmin katu 2, 00014 University of Helsinki, Finland
- 73 Université de Genève, Département de Physique Théorique and Centre for Astroparticle Physics, 24 quai Ernest-Ansermet, CH-1211 Genève 4, Switzerland
- 74 Department of Physics, P.O. Box 64, 00014 University of Helsinki, Finland
- 75 Helsinki Institute of Physics, Gustaf Hållströmin katu 2, University of Helsinki, Helsinki, Finland
- 76 Centre de Calcul de l'IN2P3/CNRS, 21 avenue Pierre de Coubertin 69627 Villeurbanne Cedex, France
- 77 Laboratoire d'étude de l'Univers et des phénomènes eXtremes, Observatoire de Paris, Université PSL, Sorbonne Université, CNRS, 92190 Meudon, France
- 78 SKA Observatory, Jodrell Bank, Lower Withington, Macclesfield, Cheshire SK11 9FT, UK
- 79 Dipartimento di Fisica "Aldo Pontremoli", Università degli Studi di Milano, Via Celoria 16, 20133 Milano, Italy
- 80 INFN-Sezione di Milano, Via Celoria 16, 20133 Milano, Italy
- 81 University of Applied Sciences and Arts of Northwestern Switzerland, School of Computer Science, 5210 Windisch, Switzerland
- 82 Universität Bonn, Argelander-Institut für Astronomie, Auf dem Hügel 71, 53121 Bonn, Germany
- 83 INFN-Sezione di Roma, Piazzale Aldo Moro, 2 - c/o Dipartimento di Fisica, Edificio G. Marconi, 00185 Roma, Italy
- 84 Dipartimento di Fisica e Astronomia "Augusto Righi" - Alma Mater Studiorum Università di Bologna, via Piero Gobetti 93/2, 40129 Bologna, Italy
- 85 Department of Physics, Institute for Computational Cosmology, Durham University, South Road, Durham, DH1 3LE, UK
- 86 Université Paris Cité, CNRS, Astroparticule et Cosmologie, 75013 Paris, France
- 87 CNRS-UCB International Research Laboratory, Centre Pierre Binetruy, IRL2007, CPB-IN2P3, Berkeley, USA
- 88 Institut d'Astrophysique de Paris, 98bis Boulevard Arago, 75014, Paris, France
- 89 Institut d'Astrophysique de Paris, UMR 7095, CNRS, and Sorbonne Université, 98 bis boulevard Arago, 75014 Paris, France
- 90 Institute of Physics, Laboratory of Astrophysics, Ecole Polytechnique Fédérale de Lausanne (EPFL), Observatoire de Sauverny, 1290 Versoix, Switzerland
- 91 Aurora Technology for European Space Agency (ESA), Camino bajo del Castillo, s/n, Urbanización Villafranca del Castillo, Villanueva de la Cañada, 28692 Madrid, Spain
- 92 Institut de Física d'Altes Energies (IFAE), The Barcelona Institute of Science and Technology, Campus UAB, 08193 Bellaterra (Barcelona), Spain
- 93 DARK, Niels Bohr Institute, University of Copenhagen, Jagtvej 155, 2200 Copenhagen, Denmark
- 94 Waterloo Centre for Astrophysics, University of Waterloo, Waterloo, Ontario N2L 3G1, Canada
- 95 Department of Physics and Astronomy, University of Waterloo, Waterloo, Ontario N2L 3G1, Canada
- 96 Perimeter Institute for Theoretical Physics, Waterloo, Ontario N2L 2Y5, Canada
- 97 Université Paris-Saclay, Université Paris Cité, CEA, CNRS, AIM, 91191, Gif-sur-Yvette, France
- 98 Centre National d'Etudes Spatiales – Centre spatial de Toulouse, 18 avenue Edouard Belin, 31401 Toulouse Cedex 9, France
- 99 Institute of Space Science, Str. Atomistilor, nr. 409 Măgurele, Ilfov, 077125, Romania
- 100 Dipartimento di Fisica e Astronomia "G. Galilei", Università di Padova, Via Marzolo 8, 35131 Padova, Italy
- 101 Institut für Theoretische Physik, University of Heidelberg, Philosophenweg 16, 69120 Heidelberg, Germany
- 102 Institut de Recherche en Astrophysique et Planétologie (IRAP), Université de Toulouse, CNRS, UPS, CNES, 14 Av. Edouard Belin, 31400 Toulouse, France
- 103 Université St Joseph; Faculty of Sciences, Beirut, Lebanon
- 104 Departamento de Física, FCFM, Universidad de Chile, Blanco Encalada 2008, Santiago, Chile
- 105 Universität Innsbruck, Institut für Astro- und Teilchenphysik, Technikerstr. 25/8, 6020 Innsbruck, Austria
- 106 Institut d'Estudis Espacials de Catalunya (IEEC), Edifici RDIT, Campus UPC, 08860 Castelldefels, Barcelona, Spain
- 107 Atlantis, University Science Park, Sede Bld 48940, Leioa-Bilbao, Spain
- 108 Institute of Space Sciences (ICE, CSIC), Campus UAB, Carrer de Can Magrans, s/n, 08193 Barcelona, Spain
- 109 Instituto de Astrofísica e Ciências do Espaço, Faculdade de Ciências, Universidade de Lisboa, Tapada da Ajuda, 1349-018 Lisboa, Portugal
- 110 Universidad Politécnica de Cartagena, Departamento de Electrónica y Tecnología de Computadoras, Plaza del Hospital 1, 30202 Cartagena, Spain

- ¹¹¹ Centre for Information Technology, University of Groningen, P.O.
Box 11044, 9700 CA Groningen, The Netherlands
- ¹¹² INFN-Bologna, Via Imerio 46, 40126 Bologna, Italy
- ¹¹³ Kapteyn Astronomical Institute, University of Groningen, PO Box
800, 9700 AV Groningen, The Netherlands
- ¹¹⁴ Infrared Processing and Analysis Center, California Institute of
Technology, Pasadena, CA 91125, USA
- ¹¹⁵ ICL, Junia, Université Catholique de Lille, LITL, 59000 Lille,
France

Appendix A: UCD catalogue

This appendix provides the details of the electronic table containing information of the UCDs analysed in this study, including both the 109 previously known and 33 newly discovered objects.

Table A.1. Content of the UCD catalogue with the first selected object as an example. This catalogue contains all the UCDs used in this work that are made available online.

Parameter	Format	Unit	Comment	Example
SHORTNAME	a14	...	Short name used in text	J0352-4910
SIMBADNAME	a30	...	Common discovery name	WISEA J035231.80-491059.4
EUCLIDNAME	a27	...	Positional IAU name	EUCL J035231.98-491058.8
OBJECT_ID	i20	...	Unique source identifier	−581332495491830038
RIGHT_ASCENSION	f11.7	deg	Right ascension (ep. ~ 2024.6)	58.1332495
DECLINATION	f11.7	deg	Declination (ep. ~ 2024.6)	−49.1830038
PMRA	f9.3	mas yr ^{−1}	Proper motion in RA	Null
PMRAERR	f9.3	mas yr ^{−1}	RA proper motion error	Null
PMDEC	f9.3	mas yr ^{−1}	Proper motion in Dec	Null
PMDECERR	f9.3	mas yr ^{−1}	Dec proper motion error	Null
FLAG_VIS	i3	...	VIS flux flag	0
FLUX_VIS_2FWHM_APER	f11.3	μJy	VIS flux at 2 FWHM aperture	0.691
FLUXERR_VIS_2FWHM_APER	f11.3	μJy	VIS aperture photometry error	0.050
FLAG_Y	i3	...	Y flux flag	0
FLUX_Y_2FWHM_APER	f11.3	μJy	Y flux at 2 FWHM aperture	37.511
FLUXERR_Y_2FWHM_APER	f11.3	μJy	Y aperture photometry error	0.433
FLAG_J	i3	...	J flux flag	0
FLUX_J_2FWHM_APER	f11.3	μJy	J flux at 2 FWHM aperture	56.488
FLUXERR_J_2FWHM_APER	f11.3	μJy	J aperture photometry error	0.481
FLAG_H	i3	...	H flux flag	0
FLUX_H_2FWHM_APER	f11.3	μJy	H flux at 2 FWHM aperture	33.353
FLUXERR_H_2FWHM_APER	f11.3	μJy	H aperture photometry error	0.298
FWHM	f4.1	arcsec	Full width at half maximum	1.2
POINT_LIKE_PROB	f4.2	...	Source point-like probability	0.18
ELLIPTICITY	f4.2	...	SExtractor source ellipticity	0.19
POSITION_ANGLE	f5.1	deg	Position angle of the source	11.0
DATALABS_PATH	a35	...	ESA datalabs spectrum file path	/data/euclid_q1/Q1_R1/SIR/102020531
DIST	f7.1	pc	Spectroscopic distance	32.4
DISTERR	f7.1	pc	Spectroscopic distance error	11.4
SPT	a10	...	SpT from various sources	T7.0
SPECTRASNR	f7.2	...	Spectra signal-to-noise	15.32
SPECTRAPIXELS	i4	...	Spectrum good pixels number	321

Appendix B: Choice of flux for point–source photometry

In this appendix, we compare the various *Euclid* fluxes to find the best choice to determine magnitudes for pointlike sources. Figure B.1 illustrates the difference of various *Euclid* magnitudes with magnitudes in *I*, *Y*, *J*, and *H* bands from the DES and VHS surveys. Points of different colours denote the distinct flux aperture options, as indicated in the legend, along with the standard deviation of each distribution.

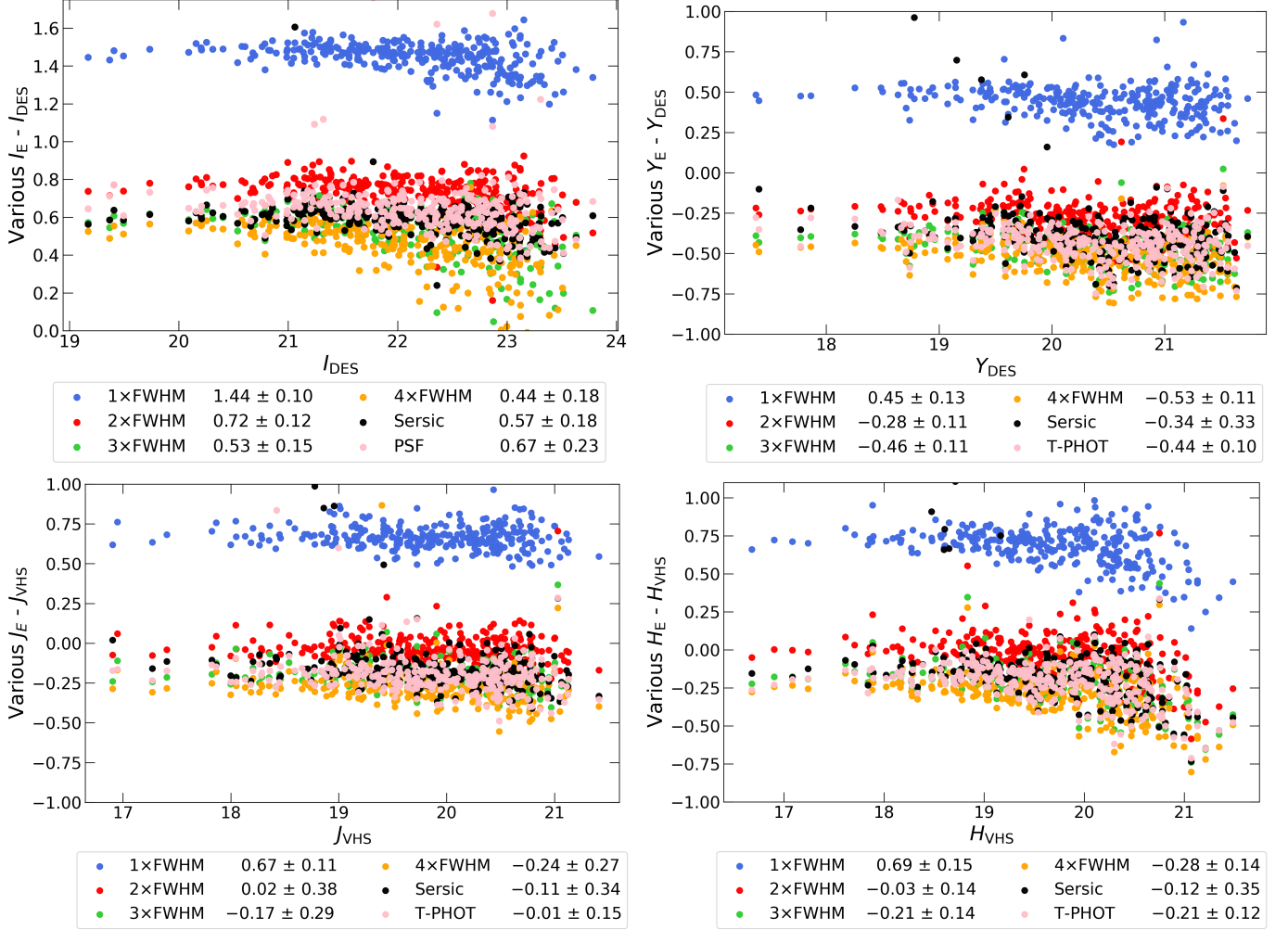


Fig. B.1. Comparison of MER magnitudes with published magnitudes for the DES objects with good spectra. Points of distinct colours represent magnitudes from various *Euclid*-derived fluxes: A-PHOT 1 × FWHM, 2 × FWHM, 3 × FWHM, and 4 × FWHM are given in blue, red, green, and yellow, respectively. Sersic is shown in black, while PSF (for VIS) and T-PHOT (for NISP) are represented in pink, see Sect. 4.1 for details. *Top*: Comparison of DES *I* and *Y* magnitudes with *Euclid* I_E and Y_E . *Bottom*: Comparison of VHS *J* and *H* magnitudes, transformed to the AB system, with *Euclid* J_E and H_E . The legend in all cases reports the mean and standard deviation of the respective comparisons.